Hund's coupling and spin-orbit interaction in the three-band Hubbard model: Anomalous mass renormalization in Sr_2RuO_4

Arun Kumar Maurya [*] and Amal Medhi [†]
Indian Institute of Science Education and Research Thiruvananthapuram, Kerala 695551, India

(Received 26 July 2022; revised 21 November 2022; accepted 6 March 2023; published 14 March 2023)

We study electronic correlation effects in the three-band Hubbard model in presence of Hund's and spin-orbit couplings using slave-spin mean-field theory. We consider three different regimes of hopping parameter values for the model on a square lattice. For orbital diagonal and isotropic hopping, we show that spin-orbit coupling (SOC), in general, enhances electronic correlations via the reduction of orbital degeneracy. In presence of Hund's coupling J, SOC tends to oppose the effect of J on electronic correlations. Considering symmetry allowed anisotropic hopping, we find that the quasiparticle weights become orbital selective in presence of interaction. The effect of J is particularly interesting for the band filling of two particles per site. Here, the Janus-faced effect of J on correlation is obtained only in the narrower band, whereas electronic correlation in the wider band get reduced by J for all values of Hubbard repulsion U. For model parameters corresponding to Sr_2RuO_4, interestingly, we find that the mass renormalizations in the bands become anomalous in presence of strong U and J. The effective mass enhancement in the wider band becomes greater compared to that in the narrower band. We show that it originates in the peculiar electronic band structure of Sr_2RuO_4, in which the spinon Fermi surface topology changes in a particular way in the presence of interactions.

DOI: 10.1103/PhysRevB.107.125131

I. INTRODUCTION

Correlated electrons in multiband systems have been a subject of intense research interests for long [1–12]. In multiband materials with orbital degeneracy, Hund's coupling J between the intra-atomic electrons gives rise to new physics absent in single band systems, such as the bad metallic behavior, itinerant ferromagnetism, etc. [5,12]. The spin-orbit coupling (SOC) is another important factor which is shown to give rise to interesting phenomenon, such as the topological insulating phases in materials [13–15]. The SOC strength λ is generally strong in materials with heavy ions. In $3d$ electron materials, electronic interaction is strong but the SOC is weak. In $4d$ and $5d$ materials, electrons are more delocalized and electron-electron interaction is weaker. At the same time, the SOC is expected to be stronger due to the heavier atoms. Therefore there is a possibility that all the three interaction scales, e.g., Hubbard repulsion U, Hund's exchange coupling J and SOC λ, come into play together in these materials and give rise to more exotic phases [16–20]. A few examples of such materials are different families of iridates with iridium in Ir^{4+} oxidation state [20–28], osmium oxides [29], materials with localized electrons due to strong correlation [30–34], etc. In materials where correlation is not strong enough so that electrons are still delocalized, the interplay between SOC and electronic correlation generally leads to different kinds of topological phases, such as Weyl semimetal [14,35,36], axion insulators [37,38], etc. On the other hand, in materials with localized electrons, SOC can lead to highly anisotropic exchange couplings favorable to the exotic spin-liquid phase [39,40]. Another particularly interesting example of a multiband material is Sr_2RuO_4 whose normal state properties bear the distinctive signatures of effects of J and λ. The material attracted considerable attention due to its unconventional superconductivity at very low temperature which was thought to be a spin-triplet superconductor though the issue still remains unresolved [41,42].

Theoretically, the interplay of electronic correlations and SOC has been studied within the multiband Hubbard model by several authors mostly using dynamical mean-field theory (DMFT) [43–50]. In the absence of SOC, the essential features of the phase diagram of the three-band Hubbard model, except for the bad metallic behavior at the band filling of $N = 2$ particles per site, is roughly understood in terms of the competition between the atomic charge gap and the kinetic energy [51]. The SOC term changes the local Hamiltonian, altering the atomic gap structure and reducing the orbital degeneracy. Therefore SOC is expected to make significant changes in the ground state phase diagram. In a detailed DMFT study, Triebl *et al.* [43] showed that for band fillings with $N = 5$ and $N = 1$ electrons per atom, the SOC enhances electronic correlations with the effect being stronger for larger values of Hund's coupling J. Opposite to this effect, at half-filling with $N = 3$, SOC makes the electronic correlations weaker. For $N = 4$, the effect of SOC is minimal unless the value of SOC is very high. Interestingly at the band filling of $N = 2$ electrons per site, where strong J enhances effective correlations at smaller U values, introduction of SOC is found to suppress this effect of J. The above overall DMFT picture notwithstanding, it is imperative to examine the physics using the slave-spin mean-field (SSMF) theory which deals with the ground state directly and takes into account the exact density of states for

[*] akmourya13@iisertvm.ac.in
[†] amedhi@iisertvm.ac.in

the lattice [7,8,52,53]. Though the formalism has been applied extensively to study the phase diagrams of various multiband Hubbard models by numerous works [7–11,51,54–56], to our knowledge it has not been applied so far to systems with spin-orbit coupling.

In this work, we undertake this task and study the paramagnetic ground state of the three-band Hubbard model in presence of both Hund's and spin-orbit couplings using the SSMF theory. We consider a square lattice and consider the model in three different regimes of hopping parameter values. One is isotropic orbital diagonal hopping between nearest-neighbor sites. In the second case, we include the next-nearest-neighbor hopping allowed by symmetry which makes bands anisotropic. Third, we consider parameter values that correspond to the real material Sr_2RuO_4. We show that, in general, in the absence of Hund's coupling, the SOC enhances electronic correlations via removal of orbital degeneracy and the consequent reduction in kinetic energy. However in the presence of J, it tends to oppose the effect of Hund's coupling on the correlations. In the case of anisotropic bands, the electronic correlations become orbital selective in presence of Hubbard repulsion U. At $N = 2$ particles per site, while J shows a Janus-faced effect [57] on correlations in the narrower bands, it reduces correlations in the wider band at all values of U. Spin-orbit coupling changes the nature of Mott transition to first order and reduces the critical interaction strength U_c drastically. For parameter values corresponding to Sr_2RuO_4, the effect of interaction is very interesting. Because of the peculiar electronic band structure of Sr_2RuO_4, the spinon Fermi surface topology changes in a particular way in presence strong U and J. It leads to the quasiparticle effective mass in the wider band getting enhanced more compared to that in the narrower band. The rest of the paper is organized as follows. In Sec. II, we introduce the model and in Sec. III, we describe the method. Results are described and discussed in Sec. IV and the final concluding remarks are given in Sec. V.

II. MODEL

We consider the following three-band Hubbard model on the square lattice appropriate for three t_{2g} orbitals per site:

$$\mathscr{H} = \mathscr{H}_{\rm t} + \mathscr{H}_{\rm int} + \mathscr{H}_{\rm SOC}. \tag{1}$$

The three t_{2g} orbitals are $d_{xz} \equiv 1$, $d_{yz} \equiv 2$, and $d_{xy} \equiv 3$. The hopping Hamiltonian is given by

$$\mathscr{H}_{\rm t} = \sum_{\substack{ij\sigma\\ mm'}} T^{ij}_{mm'}(c^\dagger_{im\sigma} c_{jm'\sigma} + \text{H.c.}) - \sum_{im\sigma} \varepsilon_{m\sigma} n_{im\sigma} \tag{2}$$

and the Hubbard-Kanamori interaction term is given by

$$\begin{aligned}\mathscr{H}_{\rm int} = {} & U \sum_{im} n_{im\uparrow} n_{im\downarrow} + U' \sum_{im\neq m'} n_{im\uparrow} n_{im'\downarrow} \\ & + U'' \sum_{\substack{m<m'\\ i\sigma}} n_{im\sigma} n_{im'\sigma} - J \sum_{im\neq m'} c^\dagger_{im\uparrow} c_{im\downarrow} c^\dagger_{im'\downarrow} c_{im'\uparrow} \\ & + J \sum_{im\neq m'} c^\dagger_{im\uparrow} c^\dagger_{im\downarrow} c_{im'\downarrow} c_{im'\uparrow}. \end{aligned} \tag{3}$$

The atomic spin-orbit coupling (SOC) term is given by

$$\mathscr{H}_{\rm SOC} = \lambda \sum_i \mathbf{L}_i \cdot \mathbf{S}_i, \tag{4}$$

where $c^\dagger_{im\sigma}$ ($c_{im\sigma}$) creates (annihilates) an electron with spin σ at site i, and orbital $m \in \{1, 2, 3\}$. The quantities $T^{ij}_{mm'}$-s are the hopping matrix elements. The parameter U is intraorbital Hubbard interaction strength and J is Hund's exchange coupling which favors atomic states with maximum total spin and orbital angular momenta. $\varepsilon_{m\sigma}$ is the atomic energy level for orbital $m\sigma$. The Hamiltonian becomes rotationally invariant to both spin and orbital degrees of freedom by choosing $U' = U - 2J$ and $U'' = U - 3J$. The Hamiltonian describes a system where the degenerate d-orbital in the isolated atoms undergo a crystal field splitting into a higher energy level e_g doublet with $d_{3z^2-r^2}$, and $d_{x^2-y^2}$ symmetry and a lower one t_{2g} triplet with d_{xy}, d_{yz}, and d_{zx} symmetry. At low temperatures, the d-orbital electrons occupy the lower t_{2g} levels and the upper e_g levels can be neglected since they lie higher in energy. There are also effects of lattice deformation, which we neglect here for simplicity. Here we consider the dynamics of electrons in this lower t_{2g} manifold where electrons hop among the t_{2g} orbitals. The angular momentum operator $\mathbf{L}_0$ projected into the t_{2g} subspace $\mathbf{L} = \mathscr{P}_{t_{2g}}(-\mathbf{L}_0)\mathscr{P}_{t_{2g}}$ behaves as effective angular momentum operator with $l = 1$. We consider the spin-orbit coupling (SOC) within this subspace. The SOC further splits the t_{2g} triplet into lower quartet ($j = 3/2$) and upper doublet ($j = 1/2$), which are spin-orbit coupled fourfold and twofold degenerate orbitals, respectively. Here we work within the basis $\{|yz\uparrow\rangle, |yz\downarrow\rangle, |zx\uparrow\rangle, |zx\downarrow\rangle, |xy\uparrow\rangle, |xy\downarrow\rangle\}$ in which the SOC term in the Hamiltonian given by

$$\mathscr{H}_{\rm SOC} = \lambda \sum_i \mathbf{L}_i \cdot \mathbf{S}_i \equiv \sum_{i\alpha\beta} \lambda_{\alpha,\beta} c^\dagger_{i\alpha} c_{i\beta}. \tag{5}$$

The $\lambda_{\alpha,\beta}$ matrix elements are given by

$$\boldsymbol{\lambda} = \frac{\lambda}{2} \begin{pmatrix} 0 & 0 & i & 0 & 0 & -1 \\ 0 & 0 & 0 & -i & 1 & 0 \\ -i & 0 & 0 & 0 & 0 & i \\ 0 & i & 0 & 0 & i & 0 \\ 0 & 1 & 0 & -i & 0 & 0 \\ -1 & 0 & -i & 0 & 0 & 0 \end{pmatrix}. \tag{6}$$

The above corresponds to a SOC energy of λ for the $j = 1/2$ doublet terms and that of $-\lambda/2$ for the $j = 3/2$ quadruplet terms in the diagonal spin-orbit coupled basis. The hopping matrix elements in the above allowed by symmetry have the form [19] as shown in Table I. Regarding the physical values of various parameters, it varies significantly among different classes of materials [57,58]. In $3d$ transition metal oxides, typical values of Hubbard interaction and Hund's coupling are $U \sim 3$ eV and $J \sim 0.4$ eV while the bandwidth is $W \sim 1$ eV. On the other hand, SOC is very weak, $\lambda \sim 0.05$ eV [45]. This translates to values, $U/W \sim 3$, $J/U \sim 0.15$, $\lambda/W \sim 0.01$ for these materials. In $4d$ oxides, U and J are slightly smaller while SOC is slightly stronger. Typical estimates are $U/W \sim 2$,

TABLE I. Hopping amplitudes of the model allowed by symmetry [19].

	xz-xz	*yz-yz*	*xy-xy*	*xz-yz*
$T^{\pm1,0,0}$	$-t_2$	$-t_3$	$-t$	0
$T^{0,\pm1,0}$	$-t_3$	$-t_2$	$-t$	0
$T^{\pm1,\pm1,0}$	0	0	$-t_1$	$-t_4$
$T^{\pm1,\mp1,0}$	0	0	$-t_1$	$-t_4$

$J/U \sim 0.1$ and $\lambda/W \sim 0.05$. In $5d$ materials, Coulomb interactions are much smaller compared to the bandwidth but SOC is strong. Again typical estimates are $U/W \sim 0.5$, $J/U \sim 0.07$. SOC can be as high as $\lambda/W \sim 0.1$. The values of these parameters considered here in our calculations are broadly representative of the above range of values, though do not exactly correspond any one particular material. However, for Sr_2RuO_4 which is separately dealt with in Sec. IV C, the parameter values considered are close to the actual parameter values for the material.

III. SLAVE-SPIN MEAN-FIELD METHOD WITH SPIN-ORBIT COUPLING

The slave-spin mean-field (SSMF) method used here has been described in detail elsewhere [7,8,51,52,54]. Here we outline the main steps highlighting the additional term that comes due to spin-orbit interaction. In the slave-spin formalism, the physical electronic Hilbert space is mapped into an enlarged Hilbert space of fermions (spinons) and auxiliary spin-1/2 (slave-spin) variables. Defining $\alpha \equiv m\sigma$, we write the physical electron states in terms of spinon and slave-spin variables as follows:

$$\begin{aligned} |n_{i\alpha}=0\rangle &\Rightarrow |n^f_{i\alpha}=0, S^z_{i\alpha}=-1/2\rangle, \\ |n_{i\alpha}=1\rangle &\Rightarrow |n^f_{i\alpha}=1, S^z_{i\alpha}=+1/2\rangle, \end{aligned} \tag{7}$$

where $n^f_{i\alpha} = f^\dagger_{i\alpha} f_{i\alpha}$ is the number operator for spinons (quasiparticles). $S^z_{i\alpha}$ is the slave-spin variable coupled to the spin-orbital. The enlarged local Hilbert space also contains the unphysical states which can be eliminated by imposing the constraint, $n^f_{i\alpha} = S^z_{i\alpha} + \frac{1}{2}$. The electron operators are decomposed accordingly as $c_{i\alpha} = f_{i\alpha} O_{i\alpha}$ and $c^\dagger_{i\alpha} = f^\dagger_{i\alpha} O^\dagger_{i\alpha}$. In the Z_2 representation, $O_{i\alpha} = S^-_{i\alpha} + g_{i\alpha} S^+_{i\alpha}$. After the slave-particle transformation of the electron operators, the Hamiltonian of Eq. (1) becomes

$$\begin{aligned} \mathscr{H} = &\sum_{ij,\alpha\beta} T_{i\alpha,j\beta} (O^\dagger_{i\alpha} O_{j\beta} f^\dagger_{i\alpha} f_{j\beta} + \text{H.c.}) - \sum_{i\alpha} \varepsilon_\alpha n^f_{i\alpha} \\ &+ \sum_{i\alpha\beta} \lambda_{\alpha,\beta} O^\dagger_{i\alpha} O_{i\beta} f^\dagger_{i\alpha} f_{i\beta} - \mu \sum_{i\alpha} n^f_{i\alpha} \\ &- \sum_{i\alpha} h_{i\alpha} \left[n^f_{i\alpha} - \left(S^z_{i\alpha} + \frac{1}{2} \right) \right] + \mathscr{H}^S_{\text{int}}, \end{aligned} \tag{8}$$

where the chemical potential μ and Lagrange multipliers $h_{i\alpha}$ are introduced and the form of the interaction term $\mathscr{H}^S_{\text{int}}$ is defined as

$$\begin{aligned} \mathscr{H}^S_{\text{int}} \equiv &U \sum_{im} \overline{S^z_{im\uparrow} S^z_{im\downarrow}} + U' \sum_{im\neq m'} \overline{S^z_{im\uparrow} S^z_{im'\downarrow}} \\ &+ (U'-J) \sum_{im<m'\sigma} \overline{S^z_{im\sigma} S^z_{im'\sigma}} \\ &- J \sum_{im\neq m'} S^+_{im\uparrow} S^-_{im\downarrow} S^+_{im'\downarrow} S^-_{im'\uparrow} \\ &+ J \sum_{im\neq m'} S^+_{im\uparrow} S^+_{im\downarrow} S^-_{im'\downarrow} S^-_{im'\uparrow}, \end{aligned} \tag{9}$$

where $\overline{S^z_{i\alpha} S^z_{i\alpha'}} = S^z_{i\alpha} S^z_{i\alpha'} + (S^z_{i\alpha} + S^z_{i\alpha'})/2$. By approximating the ground state as $|\Psi\rangle = |\Psi_f\rangle|\Psi_S\rangle$, the effective spinon and slave-spin Hamiltonians $\mathscr{H}_f = \langle\Psi_S|\mathscr{H}|\Psi_S\rangle$ and $\mathscr{H}_S = \langle\Psi_f|\mathscr{H}|\Psi_f\rangle$ are given by

$$\begin{aligned} \mathscr{H}_f = &\sum_{ij,\alpha\beta} T_{i\alpha,j\beta} (B_{i\alpha,j\beta} f^\dagger_{i\alpha} f_{j\beta} + \text{H.c.}) \\ &+ \sum_{i\alpha\beta} \lambda_{\alpha,\beta} B_{i\alpha,i\beta} f^\dagger_{i\alpha} f_{i\beta} \\ &- \sum_{i\alpha} (\mu + \varepsilon_\alpha + h_{i\alpha}) n^f_{i\alpha}, \end{aligned} \tag{10}$$

$$\begin{aligned} \mathscr{H}_S = &\sum_{ij,\alpha\beta} T_{i\alpha,j\beta} (\chi_{i\alpha,j\beta} O^\dagger_{i\alpha} O_{j\beta} + \text{H.c.}) \\ &+ \sum_{i\alpha\beta} \lambda_{\alpha,\beta} \chi_{i\alpha,i\beta} O^\dagger_{i\alpha} O_{i\beta} \\ &+ \sum_{i\alpha} h_{i\alpha} \left(S^z_{i\alpha} + \frac{1}{2} \right) + \mathscr{H}^S_{\text{int}}, \end{aligned} \tag{11}$$

where $\chi_{i\alpha,j\beta} = \langle\Psi_f| f^\dagger_{i\alpha} f_{j\beta} |\Psi_f\rangle$ and $B_{i\alpha,j\beta} = \langle\Psi_S| O^\dagger_{i\alpha} O_{j\beta} |\Psi_S\rangle$ are the mean-field parameters to be calculated by solving the spinon and slave-spin Hamiltonians self-consistently. We use single site approximation to solve the slave-spin Hamiltonian, where we take $O^\dagger_{i\alpha} O_{j\beta} \approx O^\dagger_{i\alpha} \Phi_\beta$. The parameter Φ_β is given by $\langle O_{j\beta}\rangle$, and $B_{i\alpha,j\beta}$ becomes $\Phi^*_\alpha \Phi_\beta$. The quasiparticle (QP) weight is given by $Z_\alpha = |\Phi_\alpha|^2$. The quantity signifies the degree of charge fluctuation in the system and forms an important parameter in the theory. It also determines the effective mass enhancement of the quasiparticles due to interaction which is given by $m^* = m_0/Z_\alpha$. The parameter has the value $Z_\alpha = 1$ in the noninteracting case, decreases with increasing U and vanishes in the Mott insulating state. The spinon and slave-spin Hamiltonians take the following forms:

$$\begin{aligned} \mathscr{H}_f = &\sum_{ij,\alpha\beta} T_{i\alpha,j\beta} B_{\alpha,\beta} \left(f^\dagger_{i\alpha} f_{j\beta} + \text{H.c.} \right) + \sum_{i\alpha\beta} \lambda_{\alpha,\beta} B_{\alpha,\beta} f^\dagger_{i\alpha} f_{i\beta} \\ &- \sum_{i\alpha} (\mu + \varepsilon_\alpha + h_{i\alpha}) n^f_{i\alpha}, \end{aligned} \tag{12}$$

$$\begin{aligned} \mathscr{H}_S = &\sum_{i\alpha} (\eta_{i\alpha} O^\dagger_{i\alpha} + \text{H.c.}) + \sum_{i\alpha\beta} \lambda_{\alpha,\beta} \chi_{i\alpha,i\beta} O^\dagger_{i\alpha} O_{i\beta} \\ &+ \sum_{i\alpha} h_{i\alpha} \left(S^z_{i\alpha} + \frac{1}{2} \right) + \mathscr{H}^S_{\text{int}}, \end{aligned} \tag{13}$$

where $\eta_\alpha = \sum_{j\beta} T_{i\alpha,j\beta} \chi_{i\alpha,j\beta} \Phi_\beta$.

As mentioned above, the theory introduces the unknown gauge factors $g_{i\alpha}$ through the definition $O_{i\alpha} = S^- + g_{i\alpha}S^+$. The gauge factors are determined from the condition that the slave-spin method yields the correct solution in the noninteracting limit ($U = J = 0$). Particularly, we must have $Z_{i\alpha} = 1$ in this limit. In the absence of the SOC term, the noninteracting slave-spin Hamiltonian $\mathscr{H}_S^0$ can be solved easily and it gives the following expression for gauge factors [8,52,59]:

$$g_{i\alpha} = \frac{1}{\sqrt{n_\alpha^0\left(1-n_\alpha^0\right)}} - 1; \quad n_\alpha^0 = \left\langle \Psi_f^0 \middle| n_{i\alpha}^f \middle| \Psi_f^0 \right\rangle. \tag{14}$$

However, in the presence of the SOC term, the slave-spin Hamiltonian $\mathscr{H}_S^0$ is off-diagonal in the spin-orbital index α and we need to solve the Hamiltonian,

$$\mathscr{H}_S^0 = \sum_{i\alpha}(\eta_{i\alpha}O_{i\alpha}^\dagger + \text{H.c.}) + \sum_{i\alpha\beta}\lambda_{\alpha,\beta}\chi_{i\alpha,i\beta}O_{i\alpha}^\dagger O_{i\beta} + \sum_{i\alpha}h_{i\alpha}\left(S_{i\alpha}^z + \frac{1}{2}\right) \tag{15}$$

and determine $g_{i\alpha}$-s by requiring that $Z_{i\alpha} = 1$. We do this numerically here, which brings about an additional complexity in the calculations in presence of SOC. Also the noninteracting solution may lead to a nonzero value for the Lagrange multipliers $h_{i\alpha}$. This introduces an external orbital potential in the spinon Hamiltonian and changes the spinon ground state even in the noninteracting limit. To nullify the effect, the spinon Hamiltonian is modified by subtracting the extra potential from the chemical potential term. With all the ingredients in place, we solve the self-consistent equations and obtain the mean-field parameters of the theory.

IV. RESULTS

Here, we study the paramagnetic phase diagram of the model as a function of Hubbard interaction U, Hund's exchange coupling J, and spin-orbit coupling λ. We consider two different forms of hopping. One is orbital diagonal isotropic hopping and another is anisotropic hopping allowed by the symmetry and with parameter values that correspond to Sr_2RuO_4 [19]. Before discussing the results, it is worthwhile to examine the local Hamiltonian for a single site which can be written as

$$\mathscr{H}_{\text{int}} = \frac{(U-3J)}{2}\mathbf{N}(\mathbf{N}-1) - 2J\mathbf{S}^2 - \frac{J}{2}\mathbf{L}^2 + \frac{5}{2}J\mathbf{N} + \lambda\sum_i \mathbf{L}_i\cdot\mathbf{S}_i, \tag{16}$$

where $\mathbf{N}$, $\mathbf{S}$, and $\mathbf{L}$ are the operators for the total particle number, spin, and orbital angular momentum, respectively. The ground state energy and degeneracy of the Hamiltonian corresponding to the different number of particles are listed elsewhere [50]. We can obtain the atomic gap for a given N by using the relation,

$$\Delta_{\text{at}}(N) = E_0(N+1) + E_0(N-1) - 2E_0(N). \tag{17}$$

It is important to look at the atomic gap structure, as the phase diagram of the model crucially depends upon the competition between the atomic gap and kinetic energy. In the following, the values of λ and J are normalized with nearest-neighbor hopping parameter t and Hubbard interaction U, respectively.

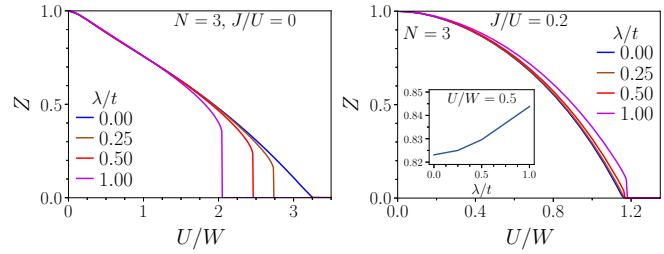

FIG. 1. Isotropic bands at half-filling. (a) The QP weight Z as a function of U/W for different values of SOC strength λ shown in the figure. Hund's coupling $J/U = 0$. (b) Same as the previous figure, but at $J/U = 0.2$. The inset in the second figure shows the increase of Z with λ at a fixed U.

A. Isotropic hopping

First, we consider the model with isotropic hopping between nearest-neighbor sites. That is we set $t = t_2 = t_3$ and $t_1 = t_4 = 0$ (Table I), and consider the model at integer band fillings. We examine the phase diagram as a function of U, J and SOC parameter λ. Solving the spinon and slave-spin Hamiltonians of Eqs. (12) and (13) self-consistently, we calculate the quasiparticle (QP) weight Z_α as a function of U for different J and λ. In this case, the quasiparticle weight Z_α is independent of the spin-orbital index α and hence we drop it in the following discussion.

The SSMF results for the model in the absence of λ are well known [51,52]. At any integer filling, the ground state is paramagnetic metallic at smaller U. The QP weight Z decreases with increasing U and vanishes continuously at a critical U_c, beyond which the state is Mott insulating. At half-filling ($N = 3$), introducing Hund's coupling J reduces the U_c value drastically. This happens as the atomic gap, $\Delta_{\text{at}} = U + 2J$ at this filling increases with J and the energy cost for charge transfer becomes larger. The half-filling results in the presence of λ are shown in Fig. 1 where we plot Z as a function of U/W (W is the noninteracting bandwidth) for various λ. The left figure shows that as soon as SOC is introduced at $J = 0$, the transition to the Mott insulating becomes first order. The QP weight vanishes abruptly at a critical U_c which decreases with increasing λ. Thus λ enhances the effect of correlation in the strong coupling regime. If we look at the atomic gap in Eq. (17), we find that Δ_{at} in this case is independent of λ. However, SOC splits the three degenerate band into a twofold degenerate ($j = 3/2$) and a nondegenerate ($j = 1/2$) orbitals and thus reduces the net kinetic energy. Therefore the effective correlation in this case gets enhanced via reduction in kinetic energy. The effect of λ in presence of J is qualitatively different [Fig. 1(b)]. With nonzero J, the U_c value already gets diminished much due to the increase in Δ_{at} with J. Introducing λ here slightly decorrelates the system with Z showing a mild increase with λ as shown in the inset of Fig. 1(b).

For the band filling $N = 2$, Hund's coupling J has very interesting consequences to the phase diagram [57]. At smaller

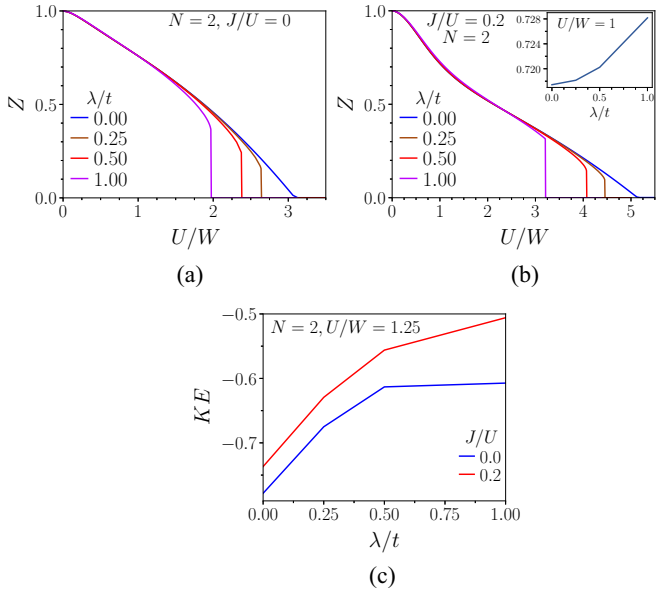

FIG. 2. Isotropic bands for $N = 2$ particles per site. (a) and (b) show Z as a function of U/W for different values of λ at $J/U = 0$ and 0.2, respectively. The inset in the second figure shows the increase of Z with λ at a fixed U. (c) Effect of λ on the kinetic energy (KE). KE drops as λ is increased due to lifting of degeneracy.

U, J correlates the system more and gives rise to the bad metallic phase. At larger U, it reduces effective electronic correlation and pushes U_c to higher values. Now if we introduce SOC at $J = 0$, we find the result to be similar to that obtained in case of $N = 3$. As shown in Fig. 2(a), the QP weight Z vanishes abruptly at a lower U_c value in presence of λ and the transition to the Mott insulating state becomes first order in nature. Similar effect of λ is observed for the $J > 0$ case also as shown in Fig. 2(b). As mentioned before, this happens due to the removal of orbital degeneracy by the SOC. In order to see this, in Fig. 2(c), we plot the kinetic energy (per site) as a function of SOC strength λ for the two values of J. The figure clearly shows the drop in kinetic energy or charge fluctuation as λ is increased. Coming back to the plot in Fig. 2(b), the effect of λ here is very interesting. The figure shows that in this case, the SOC indeed opposes the Janus-faced effect of J on the electronic correlation mentioned above. At lower U, λ pushes Z slightly up as shown in the inset of Fig. 2(b), while it brings U_c down drastically from much larger values in the absence of λ. It happens because at this filling, λ raises the atomic gap Δ_{at} as well as lowers the kinetic energy. Both these effects help in enhancing the correlations. At the filling of $N = 4$, we again find a similar effect of λ on quasiparticle weight, e.g., SOC reduces U_c in the strong coupling regime while it slightly enhances Z at moderate U. This observation agrees qualitatively with the DMFT results in Refs. [43,50]. However, it is important to mention that there are strong qualitative differences between the moderate U metallic phases at $N = 2$ and $N = 4$ [50]. For instance, the local susceptibilities show distinctly different behavior at these two fillings owing to the different values of total angular momentum J below and above half-filling. We do not see the above effect here as the frequency dependent quantities are not accessible in our method. Also at fillings $N = 1$ and $N = 5$, we find the effects to be qualitatively similar to the half-filling $J = 0$ case.

A few remarks are in order here. The reduction of critical interaction U_c by SOC in the results above appears somewhat drastic. We think this could be rather an artifact of the single-site SSMF theory than an actual physical effect. In the single-site approximation of SSMF theory, the spinon kinetic energy gets renormalized essentially by the QP weight Z instead of by the slave-particle kinetic energy, which is an approximation. A consequence of this is that as soon as system enters the Mott phase, it abruptly loses all the kinetic energy and goes to the atomic limit which is an unphysical feature. Its artifact will have its presence even in the metallic side and likely more pronounced near the Mott transition point. This has been mentioned earlier also in studies using other single-site slave-particle theories [60]. Thus it is the inaccuracies of the method in estimating the normalization of kinetic energy near the Mott transition that is likely cause for the above result.

B. Anisotropic hopping

In the previous section, we considered orbital diagonal hopping between the nearest neighbor sites with uniform strength. Here we consider also the hopping between next-nearest-neighbor (NNN) sites. The symmetry of the t_{2g} orbital restricts NNN hopping between xy-xy orbitals (t_1) and xz-yz orbitals (t_4) only, as given in Table I. Here we take $t = t_1 = t_2 = t_3 = 1$ and $t_4 = 0$. Consequently the hopping between xy-xy orbitals becomes anisotropic and the bandwidth of the xy ($m = 3$) band becomes larger. The orbital selective behavior in the multiband Hubbard model in presence of bands of unequal widths or different orbital energies have been studied extensively in the literature [7,61–65]. It has been shown that, in general, the electrons in these nonequivalent bands are localized to different degrees by electron-electron interaction. The curves of quasiparticle weights Z_m versus U get split with respect to the band index m. Z_m becomes smaller for the narrower band. Depending on the model parameter values, the Z_m values may vanish at the same U or at different values of critical interaction U_c giving rise to the orbital selective Mott transition (OSMT). Hund's coupling J is generally found to amplify the orbital selective behavior. For $J = 0$, the atomic Hamiltonian has the full SU(4) symmetry and the orbital fluctuations are high resulting in weaker orbital selective behavior. J reduces this symmetry and suppresses the orbital fluctuations due to which it is easier for the electrons in different bands to sustain different degrees of charge fluctuations. For example, in the two-band Hubbard model with unequal bandwidths, the bands undergo a common Mott transition unless the difference between the bandwidths exceeds a threshold value [7]. This threshold comes down with increasing J promoting the orbital selective behavior. Here we are interested to see how spin orbit coupling alters the scenario. As mentioned above, for our model parameters, the bandwidths of the $m = 1,\ 2$ bands are same but smaller than that of the $m = 3$ band. Since the QP weight becomes orbital dependent but remains spin independent, we denote it by Z_m. First, we show the results at half-filling. In the absence

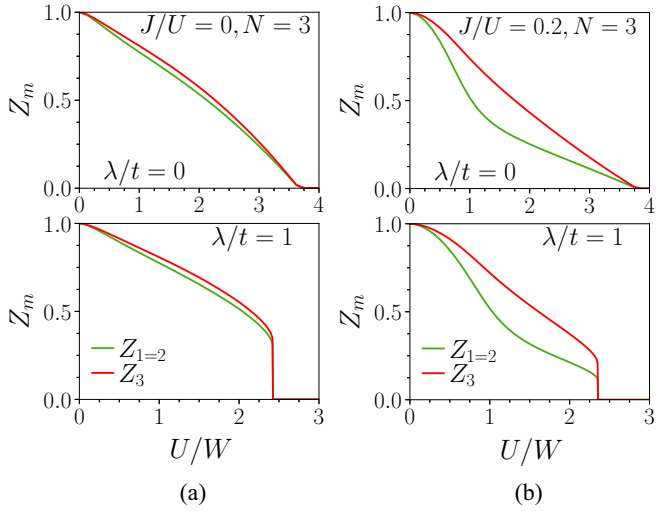

FIG. 3. Anisotropic bands at half-filling. (a) QP weight Z_m ($m = 1, 2, 3$) as a function of U/W at $J = 0$ for two values of λ, e.g., $\lambda/t = 0$ (top) and $\lambda/t = 1$ (bottom). (b) Same as the previous, but at $J/U = 0.2$.

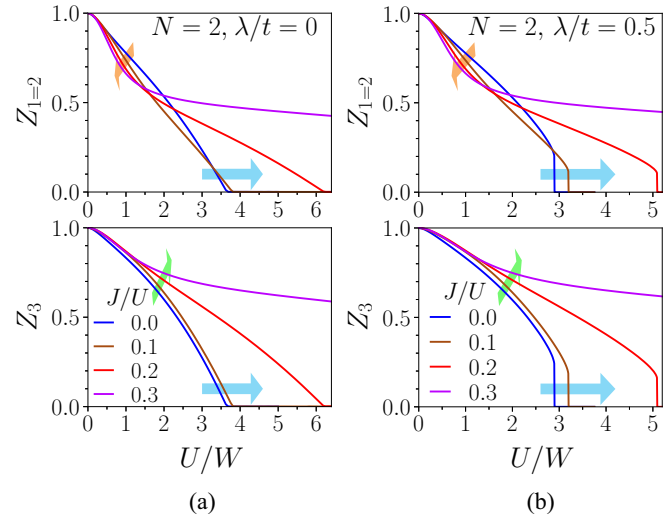

FIG. 4. Anisotropic bands at $N = 2$ particles per site. (a) QP weight Z_m as a function of U/W for different values of J/U shown in figure at $\lambda/t = 0$. (b) Same as the previous but at $\lambda/t = 0.5$. The arrows show the general trend of how J affects the electronic correlations.

of λ, the results agree with the findings in the above studies. In Fig. 3, we show the Z_m versus U curves for two different values of each parameters J and λ. As mentioned above, the curves corresponding to different bandwidths get split with the introduction of onsite repulsion U and the curves for $Z_{1=2}$ corresponding to the narrower bands lie lower. Figure 3(a) in the left panel shows that the difference between $Z_{1=2}$ and Z_3 is very small for the $J = 0$ case. This occurs because of much larger orbital fluctuations in this case as the atomic multiplets with different total orbital (L) and spin (S) angular momenta are degenerate. For nonzero J ($= 0.2U$) as shown in Fig. 3(b), the splitting between the curves becomes considerably larger, especially for intermediate values of U. In this case, the lowest atomic multiplet has the maximal values of L and S. Excitation to other multiplets has an energy cost proportional to J and hence orbital fluctuations are suppressed. However in the large U limit, the Z_m values for the bands come closer again likely because the charge fluctuation in this limit is less anyway. And for the parameter values considered here, the system undergoes a common Mott transition in both the cases. The lower two figures in Fig. 3 correspond to nonzero value of λ ($\lambda/t = 1$). We see that there is no dramatic effect of λ here. Like in the isotropic case, λ increases correlations in strong coupling regime via its effect of lifting the degeneracy and reducing kinetic energy as shown before. The Mott transition, which continues to occur at a single U value, becomes first order and the U_c value get reduced sharply.

For $N = 2$ particles per site, the effect of Hund's coupling is again intricate. In the isotropic case, J has the Janus-faced effect on electronic correlations. Here, J has similar effect for the narrower bands ($m = 1, 2$). It reduces $Z_{1=2}$ for moderate U values but increases it in the strong coupling regime. However, the effect of J on the wider band ($m = 3$) is different. It increases Z_3 for all values of U. This is shown in Fig. 4 where we plot the curves for $Z_{1=2}$ and Z_3 in separate figures. In this case also, we have a common Mott transition with $Z_{1=2}$ and Z_3 vanishing at the same U value (may not be obvious in the figure). In Fig. 4(b), we show the results for a nonzero value of λ. The SOC again influences the strong coupling phase by bringing down U_c values drastically. The effects of λ at other integer fillings are found to be qualitatively similar.

C. Parameters relevant to Sr_2RuO_4

Sr_2RuO_4 is one example of a real multiband material, where all the three energy scales, e.g. the electron-electron interaction, Hund's coupling and SOC become operative simultaneously [19,41,42]. The relevant electronic degrees of freedom in the material lie in the t_{2g} orbitals of the Ru atoms filled by four electrons and its essential features can be described by the three-band Hubbard model on a square lattice. The Fermi surface consists of three sheets, a holelike α (xz, yz bands) sheet and two electronlike β (xz, yz bands) and γ (xy) sheets [66]. The hopping between the xz-xz and yz-yz orbitals are strongly one dimensional in nature and these two bands are narrower. For the wider xy band, there is also sizable hopping between next-nearest-neighbor sites and as we show here this NNN hopping has nontrivial consequences to the electronic band structure. The material attracted a lot of attention due to the observation of unconventional superconductivity at very low temperature [41]. However several aspects, including the exact nature of the pairing symmetry, role of spin-orbit interaction on the superconducting properties, etc. are still not clear [42]. The normal state above the superconducting transition temperature behaves as a two-dimensional correlated Fermi liquid [67]. The strong correlation in the system in spite of its Hubbard interaction U being of moderate strength has been shown to be a consequence of relatively stronger Hund's coupling J [68]. The spin-orbit coupling in the material though not very strong, has interesting consequences to the Fermi surface topology and to the dynamical properties [19,42,69]. Another interesting property is the observed differential mass enhancements of the electron quasiparticles in

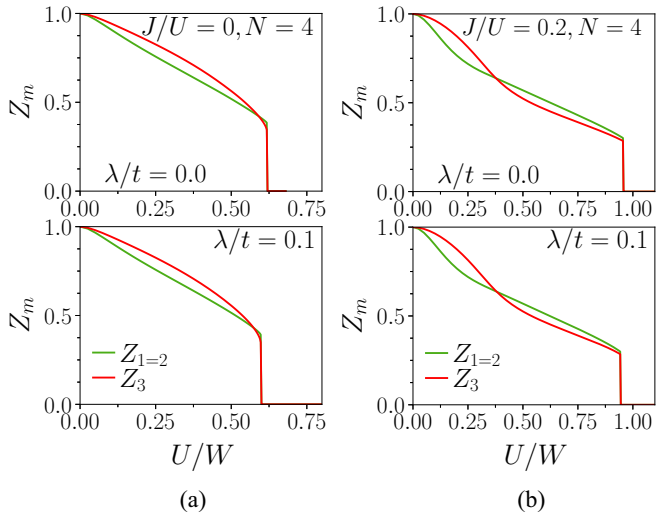

FIG. 5. Bands corresponding to Sr_2RuO_4 parameters. (a) QP weight Z_m as a function of U/W for two different values of λ at $J/U = 0$. The upper (lower) figure corresponds to $\lambda = 0$ (0.1) (b) Same as the previous but at $J/U = 0.2$. In this case, the values of QP weight for the bands change order at large U.

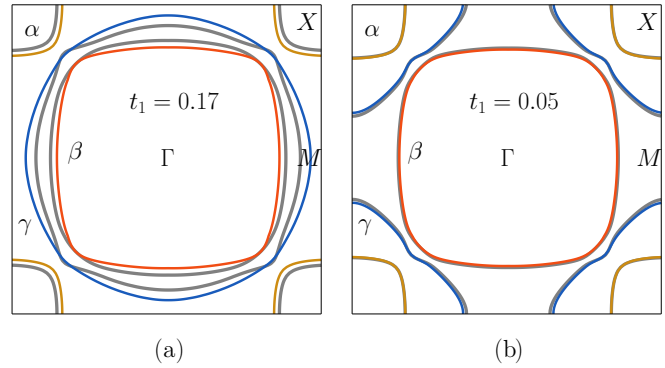

FIG. 6. Spinon Fermi surface (FS) in Sr_2RuO_4 at two different values of U in each figure. The gray lines correspond to noninteracting bands at $U = 0$ and the colored lines correspond to $U/W = 0.75$ ($J/U = 0.2$). (a) The FS for $t_1 = 0.17$, the true value of the parameter. The topology of the FS changes with interaction. (b) The FS for $t_1 = 0.05$, an arbitrary small value of the parameter. In this case, the change in the FS with interaction is negligible.

different bands by electron-electron interaction. Indeed, the mass enhancement in the wider band is found to be greater [68,69] which is counterintuitive. Many of these results and understandings have been obtained by DMFT calculations at finite temperatures though a recent study [70] using numerical renormalization group method has studied the properties of the material down to zero temperature. Here we examine the scenario for the ground state within the simpler SSMF scheme.

For the quadratic part of the Hamiltonian in Eq. (1), we take the parameter values to be the same as in Ref. [19]. That is, we take hopping parameters to be $t = 0.42$, $t_1 = 0.17$, $t_2 = 0.30$, $t_3 = 0.03$, $t_4 = 0.04$ and the onsite energies $\varepsilon_m = 0.10$ for $m = 1,\ 2$ and $\varepsilon_m = 0$ for $m = 3$. We examine the properties for two values of the SOC strength, e.g., $\lambda = 0,\ 0.1$ and vary U as well as J over wider ranges of values. The above particular value of the hopping parameter t_1 (NNN hopping between the xy orbital) is crucial as it affects the band dispersion in a peculiar way. The results for quasiparticle weight Z_m for the band filling of $N = 4$ particles per site are shown in Fig. 5. The figure shows that as soon as U is introduced, the Z_m curves get split again into two groups. The overlapping curves for bands $m = 1,\ 2$ having the same bandwidth lie lower as the bandwidth is smaller. The curve for the wider band $m = 3$ lie higher. At $J = 0$ [Fig. 5(a)], the difference in the Z_m values becomes maximum at an intermediate U. However, at larger U, the curves come closer and the bands undergo a common first order Mott transition at a single U_c value. For the small value of λ ($= 0.1$) considered here, its effect appears negligible, which agrees with the results of previous studies [19,45]. Regarding the estimate of Z, it may be mentioned that methods like SSMF, rotationally invariant slave-boson (RISB) and Gutzwiller approximation underestimate the enhancement of quasiparticle renormalization compared to DMFT+CTQMC values [10,49]. For example, for $U \sim 3$ eV, $J/U \sim 0.2$, and $\lambda \sim 0.1$ eV, RISB estimate for Z is ~0.6, whereas the same value in DMFT+CTQMC is ~0.3. Our estimate for the value is also ~0.6 which agrees well with the RISB result. Figure 5(b) shows the curves for $J/U = 0.2$ which are very interesting. For smaller U, the Z_m curves start out splitting in the same order as in the previous case. However, it crosses each other at an intermediate U and the order reverses after that. Thus at larger U values, the quasiparticle weight Z_m in the wider band becomes smaller implying greater enhancement of effective mass for the band, an observation which is in agreement with previous experimental and theoretical results [68,69]. This phenomenon has been attributed to the presence of a Van Hove singularity (VHS) in the band structure close to the β sheet. We find that this comes mainly because of the particular value of NNN hopping parameter ($t_1 = 0.17$) between the xy orbitals. In the SSMF scheme, it leads to the spinon bands getting renormalized deferentially by interaction. The signature of the effect is visible in the Fermi surface (FS) of the spinon quasiparticles whose topology changes in a particular way as a function of U. In Fig. 6(a), we show the spinon FS at two different values of U. The gray lines corresponds to the noninteracting band and the colored lines correspond to a finite value of U ($= 0.75W$, $J = 0.2U$). We see that while the volumes of the α and γ sheets increase with U, the β sheet shrinks in volume compared to the FS at $U = 0$. This change in the FS topology with interaction is in qualitative agreements with previous *ab initio* calculation results [66]. Two factors are necessary for this to happen. Presence of Hund's coupling J is of course required. In addition, we find that the effect is obtained only for a small range of t_1 values around the true value. If we tweak t_1 to be too small or too large, we do not find the crossing of the Z_m curves or any appreciable effect of interaction on the FS topology. This is shown in Fig. 6(b) where we plot the FS at $t_1 = 0.05$, an arbitrary small value of the parameter. In this case, the change in the FS with interaction is negligible. This indicates that the intricate phenomenology in Sr_2RuO_4 can be attributed to some extent to its peculiar band structure features.

V. CONCLUSION

In conclusion, we studied the electron correlation effects in multiband systems in presence of Hund's coupling and spin-orbit interaction in the context of the three-band Hubbard model on a square lattice. We used the slave-spin mean-field method which works for wider range of parameter values and gives qualitatively correct results. We considered the model in three different settings as far the hopping parameters are concerned. For the model with orbital diagonal isotropic hopping, we find results that are in qualitative agreement with previous DMFT results. We find that SOC generally enhances the electronic correlations via lifting of orbital degeneracy and consequent suppression of kinetic energy. It changes the nature of Mott transition to first order and reduces the critical interaction U_c drastically. In presence of Hund's coupling J, SOC is generally found to oppose the effect of J on electronic correlations. In case of anisotropic hopping where the bands have unequal widths, the correlations show orbital selective behavior in presence of Hubbard interaction U, though the bands undergo a common Mott transition for the parameter values considered. Interestingly, for the band filling of two particles per site, the effect of J also becomes orbital selective. Here, J shows the Janus-faced effect in the narrower band while it reduces correlations in the wider band at all values of U. We also considered the model with parameter values that correspond to Sr_2RuO_4. The effect of interaction in this case is very interesting. In presence of strong U and J, the effective mass enhancement which is the inverse of the quasiparticle weight, becomes greater in the wider band which appears anomalous. The calculation suggests that this differential renormalization of the spinon bands occurs due to the particular form of the hopping parameters. For the Sr_2RuO_4 hopping parameters, the interaction changes the spinon Fermi surface topology in a significant way which does not occur if we tweak the parameters. Thus our work have thrown lights on some very interesting effects that occur as a result of interplay of electronic correlations, spin-orbit coupling, and band structure in multiband systems.

ACKNOWLEDGMENT

The authors acknowledge the HPC center, IISER Thiruvananthapuram for computing time at the Padmanabha cluster.

[1] K. Held and D. Vollhardt, Eur. Phys. J. B **5**, 473 (1998).
[2] T. Momoi and K. Kubo, Phys. Rev. B **58**, R567 (1998).
[3] R. Peters and T. Pruschke, Phys. Rev. B **81**, 035112 (2010).
[4] R. Peters, N. Kawakami, and T. Pruschke, Phys. Rev. B **83**, 125110 (2011).
[5] R. Frésard and G. Kotliar, Phys. Rev. B **56**, 12909 (1997).
[6] K. M. Stadler, Z. P. Yin, J. von Delft, G. Kotliar, and A. Weichselbaum, Phys. Rev. Lett. **115**, 136401 (2015).
[7] L. de'Medici, A. Georges, and S. Biermann, Phys. Rev. B **72**, 205124 (2005).
[8] S. R. Hassan and L. de' Medici, Phys. Rev. B **81**, 035106 (2010).
[9] L. de' Medici, J. Mravlje, and A. Georges, Phys. Rev. Lett. **107**, 256401 (2011).
[10] L. de' Medici, S. R. Hassan, M. Capone, and X. Dai, Phys. Rev. Lett. **102**, 126401 (2009).
[11] L. de' Medici, G. Giovannetti, and M. Capone, Phys. Rev. Lett. **112**, 177001 (2014).
[12] K. Stadler, G. Kotliar, A. Weichselbaum, and J. von Delft, Ann. Phys. **405**, 365 (2019).
[13] M. Z. Hasan and C. L. Kane, Rev. Mod. Phys. **82**, 3045 (2010).
[14] X. Wan, A. M. Turner, A. Vishwanath, and S. Y. Savrasov, Phys. Rev. B **83**, 205101 (2011).
[15] M. Dzero, J. Xia, V. Galitski, and P. Coleman, Annu. Rev. Condens. Matter Phys. **7**, 249 (2016).
[16] D. Pesin and L. Balents, Nat. Phys. **6**, 376 (2010).
[17] W. Witczak-Krempa, G. Chen, Y. B. Kim, and L. Balents, Annu. Rev. Condens. Matter Phys. **5**, 57 (2014).
[18] L. Du, L. Huang, and X. Dai, Eur. Phys. J. B **86**, 94 (2013).
[19] M. Kim, J. Mravlje, M. Ferrero, O. Parcollet, and A. Georges, Phys. Rev. Lett. **120**, 126401 (2018).
[20] B. J. Kim, H. Jin, S. J. Moon, J.-Y. Kim, B.-G. Park, C. S. Leem, J. Yu, T. W. Noh, C. Kim, S.-J. Oh, J.-H. Park, V. Durairaj, G. Cao, and E. Rotenberg, Phys. Rev. Lett. **101**, 076402 (2008).
[21] B. J. Kim, H. Ohsumi, T. Komesu, S. Sakai, T. Morita, H. Takagi, and T. Arima, Science **323**, 1329 (2009).
[22] J. Kim, D. Casa, M. H. Upton, T. Gog, Y.-J. Kim, J. F. Mitchell, M. van Veenendaal, M. Daghofer, J. van den Brink, G. Khaliullin, and B. J. Kim, Phys. Rev. Lett. **108**, 177003 (2012).
[23] J. Kim, A. H. Said, D. Casa, M. H. Upton, T. Gog, M. Daghofer, G. Jackeli, J. van den Brink, G. Khaliullin, and B. J. Kim, Phys. Rev. Lett. **109**, 157402 (2012).
[24] Y. Singh and P. Gegenwart, Phys. Rev. B **82**, 064412 (2010).
[25] Y. Singh, S. Manni, J. Reuther, T. Berlijn, R. Thomale, W. Ku, S. Trebst, and P. Gegenwart, Phys. Rev. Lett. **108**, 127203 (2012).
[26] H. Gretarsson, J. P. Clancy, X. Liu, J. P. Hill, E. Bozin, Y. Singh, S. Manni, P. Gegenwart, J. Kim, A. H. Said, D. Casa, T. Gog, M. H. Upton, H.-S. Kim, J. Yu, V. M. Katukuri, L. Hozoi, J. van den Brink, and Y.-J. Kim, Phys. Rev. Lett. **110**, 076402 (2013).
[27] D. Yanagishima and Y. Maeno, J. Phys. Soc. Jpn. **70**, 2880 (2001).
[28] Y. Okamoto, M. Nohara, H. Aruga-Katori, and H. Takagi, Phys. Rev. Lett. **99**, 137207 (2007).
[29] J. Yamaura, K. Ohgushi, H. Ohsumi, T. Hasegawa, I. Yamauchi, K. Sugimoto, S. Takeshita, A. Tokuda, M. Takata, M. Udagawa, M. Takigawa, H. Harima, T. Arima, and Z. Hiroi, Phys. Rev. Lett. **108**, 247205 (2012).
[30] A. Krimmel, M. Mücksch, V. Tsurkan, M. M. Koza, H. Mutka, and A. Loidl, Phys. Rev. Lett. **94**, 237402 (2005).
[31] G. Chen, L. Balents, and A. P. Schnyder, Phys. Rev. Lett. **102**, 096406 (2009).
[32] M. A. de Vries, A. C. Mclaughlin, and J.-W. G. Bos, Phys. Rev. Lett. **104**, 177202 (2010).
[33] J. P. Carlo, J. P. Clancy, T. Aharen, Z. Yamani, J. P. C. Ruff, J. J. Wagman, G. J. Van Gastel, H. M. L. Noad, G. E. Granroth, J. E. Greedan, H. A. Dabkowska, and B. D. Gaulin, Phys. Rev. B **84**, 100404(R) (2011).

[34] G. Jackeli and G. Khaliullin, Phys. Rev. Lett. **103**, 067205 (2009).
[35] W. Witczak-Krempa and Y. B. Kim, Phys. Rev. B **85**, 045124 (2012).
[36] A. A. Burkov and L. Balents, Phys. Rev. Lett. **107**, 127205 (2011).
[37] X. Wan, A. Vishwanath, and S. Y. Savrasov, Phys. Rev. Lett. **108**, 146601 (2012).
[38] A. Go, W. Witczak-Krempa, G. S. Jeon, K. Park, and Y. B. Kim, Phys. Rev. Lett. **109**, 066401 (2012).
[39] J. c. v. Chaloupka and G. Khaliullin, Phys. Rev. B **92**, 024413 (2015).
[40] S. M. Winter, Y. Li, H. O. Jeschke, and R. Valentí, Phys. Rev. B **93**, 214431 (2016).
[41] A. P. Mackenzie and Y. Maeno, Rev. Mod. Phys. **75**, 657 (2003).
[42] A. P. Mackenzie, T. Scaffidi, C. W. Hicks, and Y. Maeno, npj Quantum Mater. **2**, 40 (2017).
[43] R. Triebl, G. J. Kraberger, J. Mravlje, and M. Aichhorn, Phys. Rev. B **98**, 205128 (2018).
[44] J. Bünemann, T. Linneweber, U. Löw, F. B. Anders, and F. Gebhard, Phys. Rev. B **94**, 035116 (2016).
[45] A. Horvat, R. Žitko, and J. Mravlje, Phys. Rev. B **96**, 085122 (2017).
[46] T. Sato, T. Shirakawa, and S. Yunoki, Phys. Rev. B **91**, 125122 (2015).
[47] M. Kim, Phys. Rev. B **97**, 155141 (2018).
[48] C. Piefke and F. Lechermann, Phys. Rev. B **97**, 125154 (2018).
[49] J. I. Facio, J. Mravlje, L. Pourovskii, P. S. Cornaglia, and V. Vildosola, Phys. Rev. B **98**, 085121 (2018).
[50] A. J. Kim, H. O. Jeschke, P. Werner, and R. Valentí, Phys. Rev. Lett. **118**, 086401 (2017).
[51] A. K. Maurya, M. T. H. Sarder, and A. Medhi, J. Phys.: Condens. Matter **33**, 425603 (2021).
[52] L. de' Medici and M. Capone, in *The Iron Pnictide Superconductors,* Springer Series in Solid-State Sciences Vol. 186 (Springer, Cham, 2017), pp. 201–213
[53] R. Yu, Z. Wang, P. Goswami, A. H. Nevidomskyy, Q. Si, and E. Abrahams, Phys. Rev. B **86**, 085148 (2012).
[54] A. K. Maurya, M. T. H. Sarder, and A. Medhi, J. Phys.: Condens. Matter **34**, 055602 (2022).
[55] Y. Komijani and G. Kotliar, Phys. Rev. B **96**, 125111 (2017).
[56] A. B. Georgescu and S. Ismail-Beigi, Phys. Rev. B **96**, 165135 (2017).
[57] A. Georges, L. de Medici, and J. Mravlje, Annu. Rev. Condens. Matter Phys. **4**, 137 (2013).
[58] L. Vaugier, H. Jiang, and S. Biermann, Phys. Rev. B **86**, 165105 (2012).
[59] A. Mezio and R. H. McKenzie, Phys. Rev. B **100**, 205134 (2019).
[60] E. Zhao and A. Paramekanti, Phys. Rev. B **76**, 195101 (2007).
[61] A. Liebsch, Phys. Rev. Lett. **95**, 116402 (2005).
[62] A. Koga, N. Kawakami, T. M. Rice, and M. Sigrist, Phys. Rev. Lett. **92**, 216402 (2004).
[63] S. Biermann, L. de' Medici, and A. Georges, Phys. Rev. Lett. **95**, 206401 (2005).
[64] M. Ferrero, F. Becca, M. Fabrizio, and M. Capone, Phys. Rev. B **72**, 205126 (2005).
[65] L. de' Medici, Phys. Rev. B **83**, 205112 (2011).
[66] G. Zhang, E. Gorelov, E. Sarvestani, and E. Pavarini, Phys. Rev. Lett. **116**, 106402 (2016).
[67] C. Bergemann, A. P. Mackenzie, S. R. Julian, D. Forsythe, and E. Ohmichi, Adv. Phys. **52**, 639 (2003).
[68] J. Mravlje, M. Aichhorn, T. Miyake, K. Haule, G. Kotliar, and A. Georges, Phys. Rev. Lett. **106**, 096401 (2011).
[69] H. J. Lee, C. H. Kim, and A. Go, Phys. Rev. B **102**, 195115 (2020).
[70] F. B. Kugler, M. Zingl, H. U. R. Strand, S.-S. B. Lee, J. von Delft, and A. Georges, Phys. Rev. Lett. **124**, 016401 (2020).